Journal of Asian Earth Sciences 123 (2016) 100–110

Contents lists available at ScienceDirect

Journal of Asian Earth Sciences

journal homepage: www.elsevier.com/locate/jseaes

Magmatic–hydrothermal evolution of highly fractionated granites: Evidence from the Kuiqi miarolite in Fujian province, SE China

Lingjun Zeng [a,b], Zhiwei Bao [a], Qiang Shan [a,*], Wubin Yang [a,c], Yan Zhao [a,b], Ningbo Li [a]

[a] CAS Key Laboratory of Mineralogy and Metallogeny, Guangzhou Institute of Geochemistry, Chinese Academy of Sciences, 511 Kehua Street, Guangzhou 510640, China
[b] University of Chinese Academy of Sciences, 19 Yuquan Road, Beijing 100049, China
[c] Guangdong Provincial Key Laboratory of Mineral Physics and Materials, 511 Kehua Street, Guangzhou 510640, China

ARTICLE INFO

Article history:
Received 6 February 2016
Received in revised form 29 March 2016
Accepted 31 March 2016
Available online 11 April 2016

Keywords:
Kuiqi miarolite
Melt/fluid inclusions
magmatic–hydrothermal evolution
Volatile-rich fluid
Immiscibility

ABSTRACT

The Kuiqi miarolite, a highly evolved alkaline granite pluton, is situated in Fujian province, southeastern China. Quartz crystals from the Kuiqi miarolite contain abundant inclusions, which have preserved a complete record of the magmatic–hydrothermal evolution. Five inclusion type were identified, i.e., the melt (M-type), melt–fluid (ML-type), daughter mineral-bearing (S-type), vapor-rich (V-type), and aqueous (L-type) inclusions. Integrated petrographic, microthermometric and laser Raman spectroscopy studies demonstrate that the whole magmatic–hydrothermal evolution at Kuiqi comprises three stages, i.e., the magmatic, magmatic–hydrothermal and hydrothermal stages. The M-type inclusions (minimal trapping temperatures: ca. 710–800 °C) represent the melts entrapped at the magmatic stage of crystallization, while the occurrence of euhedral prismatic arfvedsonites in these melt inclusions indicates that the granitic magma was probably volatile-rich. At the magmatic–hydrothermal stage, both the ML-type inclusions (T_h = ca. 500–710 °C) and coexisting M- and V-type inclusions reflect the presence of late magmatic fluid circulation and melt-volatile immiscibility, exhibiting a transition toward the hydrothermal stage. At the hydrothermal stage, the pressure and temperature (700–485 °C) drop may have led to oversaturation of the primary saline fluids, resulting in the phase separation a highly saline and a volatile-rich fluid occurred, accompanied by the widespread vapor–brine immiscibility. The L-type inclusions in the miarolitic quartz display bimodal salinity distribution: The T_h and salinity of the inclusions at the bottom (L_1) miarolitic quartz are ca. 303–427 °C and ca. 6.6–17.9 wt.% NaCl equiv, respectively, while that of the inclusions at the top (L_2) are ca. 165–232 °C and ca. 0.2–5.7 wt.% NaCl equiv, respectively. This indicates a drop of fluid temperature and salinity during the miarolitic cavity formation. Moreover, the low homogenization temperatures and salinities of the L-type inclusions suggest an influx of meteoric water during the late hydrothermal evolution stage.

1. Introduction

Exsolution of hydrothermal fluids from the crystallizing magmas and ore metals percolation by vapor-rich fluids from the subsolidus magmas are critical factors in the formation of intrusion-related hydrothermal ore deposits (e.g., Audétat et al., 2008; Sillitoe, 2010). Fluid evolution in shallow intrusions and its genetic link with the commonly associated mineralization were documented in previous fluid inclusion studies (Audétat, 2015; Cathelineau et al., 1988; Hurtig et al., 2014; Roedder, 1984; Weisbrod, 1981). Compositions of the fluid phases and their evolution in many mineralization systems were well investigated through fluid inclusion studies (Fan et al., 2002, 2003; Jiang et al., 2014; Lawrence et al., 2013; Li et al., 2012; Lu et al., 2003; Poros et al., 2012; Xie et al., 2009). Fluid inclusions entrapped in crystals are by far the most representative of the fluids existed during and after crystal growth. The volatiles evolution at hydrothermal stage has been intensively investigated, however, their behavior at the magmatic–hydrothermal stages still remains equivocal (Audétat and Pettke, 2003; Audétat et al., 2008; Kamenetsky et al., 2004).

Melt inclusion studies, such as microthermometry and geochemical analysis, can unravel important magmatic processes (Audétat and Pettke, 2003; Badanina et al., 2004; Bakker and Elburg, 2006; Harris et al., 2003; Thomas et al., 2012). Exsolution of volatile phases from the magmatic melts takes place in or between the orthomagmatic- and hydrothermal regimes during

* Corresponding author.
E-mail address: qshan@gig.ac.cn (Q. Shan).

http://dx.doi.org/10.1016/j.jseaes.2016.03.023
1367-9120/

magma cooling and crystallization (Lu, 2011). This process is difficult to document, largely because of the transient and reactive nature of the volatile phases released during magmatic cooling (Kamenetsky and Kamenetsky, 2010). It is well accepted that the magmatic–hydrothermal ore deposits are formed through a complex sequence of events starting from the generation of hydrous melts in the crust and ending in the ore metals precipitation from the hydrothermal fluids (e.g., Barnes, 1997; Gruen et al., 2014; Mogdisov and Williams-Jones, 2013).

In the last two decades, the melt- and fluid inclusion approach has become more powerful with the use of modern microbeam technology (Hammerli et al., 2013; Heinrich et al., 2003; Kurosawa et al., 2003; Morales et al., 2016; Sirbescu et al., 2013). So far, the vast majority of researches have been focused on hydrothermal mineralized intrusions, whereas only a few studies dealt with the entire magmatic evolution which is important for the ore formation (Audétat et al., 2008; Frezzotti, 1992; Hansteen and Lustenhouwer, 1990; Shan et al., 2011; Shinohara, 1994; Yang and Bodnar, 1994). Miarolitic granites are commonly formed at the final stage of the magmatic evolution and minerals in the miarolitic cavities represent good record of the magmatic–hydrothermal evolution (Audétat and Pettke, 2003; Shan et al., 2011; Thomas et al., 2009). Here, we report new data from the melt/fluid inclusions in the granular/miarolitic quartz from the Kuiqi miarolite with a purpose of reconstructing the whole process of magmatic–hydrothermal evolution there.

The Kuiqi miarolite is located in Fuzhou county (Fujian province) southeastern (SE) China. It is a highly evolved alkaline granite pluton emplaced at shallow depths (Shan et al., 2014). Various inclusion assemblages, recording the temperature and pressure at different petrogenesis stages, were identified in the Kuiqi miarolite. To better understand the volatiles behavior throughout the magmatic–hydrothermal evolution, special attention is given to a systematic field observation and the study of melt-, melt–fluid- and fluid inclusions by means of microscopic petrography, microthermometric-, and laser Raman spectroscopic (LRM) analyses.

2. Geological background

Mesozoic intrusive rocks are widespread in SE China (Bai et al., 2015; Cui et al., 2013; Zhou et al., 2013), among which the occurrence of a 500 km long and 60 km wide NE-trending miarolitic alkaline granite belt, in Fuzhou county, Fujian province, is magnificent. The miarolite belt, subparallel to the coastline, occurs along the Changle-Xiamen rift and consists of around ten miarolitic complexes including the Guanshan-, Jiantian-, Guian-, Danyang-, Fuzhou-, Kuiqi- and Bijiashan pluton (Wu, 1991). These Early Cretaceous alkaline miarolites are emplaced in an active continental margin of the Cathaysia block and are commonly associated with calc-alkaline granites (Suwa et al., 1987; Wang et al., 1985) (Fig. 1).

The Fuzhou-, Danyang-, Bijiashan- and Kuiqi plutons constitute of a batholith with three intrusive phases. Based on the contact relationships and formation ages, the three intrusive phases are: first, the Fuzhou (whole-rock Rb–Sr: 104 ± 5 Ma) and Danyang (whole-rock Rb–Sr:103 ± 10 Ma) (Huang et al., 1986) plutons distribute along the batholith margin; second, the Kuiqi pluton (zircon U–Pb: ca. 101–92 Ma LA-ICP-MS) (Shan et al., 2014) at the batholith central; and third, the Bijiashan pluton (whole-rock Rb–Sr: 92 ± 9 Ma) (Huang et al., 1986) intruded both the Kuiqi and Danyang plutons (Fig. 1). The NNE-trending Kuiqi pluton, the largest pluton in the area, intruded the Upper Jurassic Nanyuan Formation volcanic rocks (Martin et al., 1994).

The Kuiqi miarolitic granite consists mainly of alkaline granite and minor biotite granite. It has high SiO_2 (71.23–77.48 wt.%) and $Na_2O + K_2O$ (7.81–9.10 wt.%) contents (Shan et al., 2014). The intrusion can be divided into three zones: the marginal-, transitional- and central zone. The marginal zone is fine grained whereas the transitional and central zones are medium-fine and medium-coarse grained granites, respectively (Fig. 2a). The central zone of the pluton is the major focus of this study.

The miarolitic granites of the central zone contain mainly perthite (60–65 vol.%), quartz (25–35 vol.%), orthoclase (5–10 vol.%), and minor arfvedsonite (1–5 vol.%). The perthite is commonly subhedral, showing perthitic texture (Fig. 2c). The quartz is subhedral to anhedral, commonly graphically intergrew with perthite and orthoclase. The arfvedsonite is interstitial or included inside quartz or perthite (Fig. 2d).

Based on the field, hand specimen and microscopic petrography observing, the arfvedsonite, and accidental mineral such as zircon and magnetite crystalized first, then orthoclase, perthite and quartz. The quartz of miarolitic cavity is the last crystallized mineral.

Miarolitic cavities in the Kuiqi miarolities vary in size from several millimeters to decimeters (Fig. 2b), and are spherical to ellipsoidal in shape. They exhibit irregular forms (containing quartz, orthoclase and arfvedsonite), and the rims commonly show granophyric texture.

3. Analytical methods

3.1. Sampling

Samples used for the melt/fluid inclusion study were collected from the miarolitic granite and cavities in the central part of the Kuiqi pluton. Petrography of the inclusions from 85 thick sections (300 μm) were carefully studied under transmitted light microscopes, after which representative sections were selected for microthermometry (30 thick sections) and laser Raman spectroscopy (10 thick sections) analyses.

3.2. Microthermometry

Microthermometric studies of fluid inclusions were carried out on a Linkam THM 600 heating-freezing stage at the Key Laboratory of Mineralogy and Metallogeny, Guangzhou Institute of Geochemistry, Chinese Academy of Sciences (GIGCAS). Thermocouples were calibrated in the range of −196 °C to 600 °C using synthetic fluid inclusions. The precision of temperature measurement is ±0.1 °C between 25 °C and 400 °C, and ±2 °C for temperature above 400 °C. The heating rate was generally 0.2–5 °C/min during the process of fluid inclusion test, but reduced to 0.1 °C/min near the freezing point, and 0.2–0.5 °C/min near the homogenization temperature on purpose of accurately recording the phase transformation process. Microthermometric studies of melt–fluid/melt inclusions were carried out on a Linkam TS1400XY heating stage (Esposito et al., 2012). Before each run of the experiment, the heating was calibrated using the melting temperature of NaCl (810 °C). The difference between the known melting temperatures of the calibration standards and the measured temperatures of the inclusions was controlled to be <15 °C.

3.3. Laser Raman microspectroscopy

Vapor- and solid phase compositions of individual inclusion were measured using the HORIBA XploRA Plus Laser Raman microspectroscopy at the Key Laboratory of Mineralogy and Metallogeny, GIGCAS. An Ar ion laser operating at 5 mW was used to produce the excitation wavelength of 532 nm line. The scanning range of spectra was set between 100 and 4200 cm^{-1} with an accumulation time of 8 s for each scan.

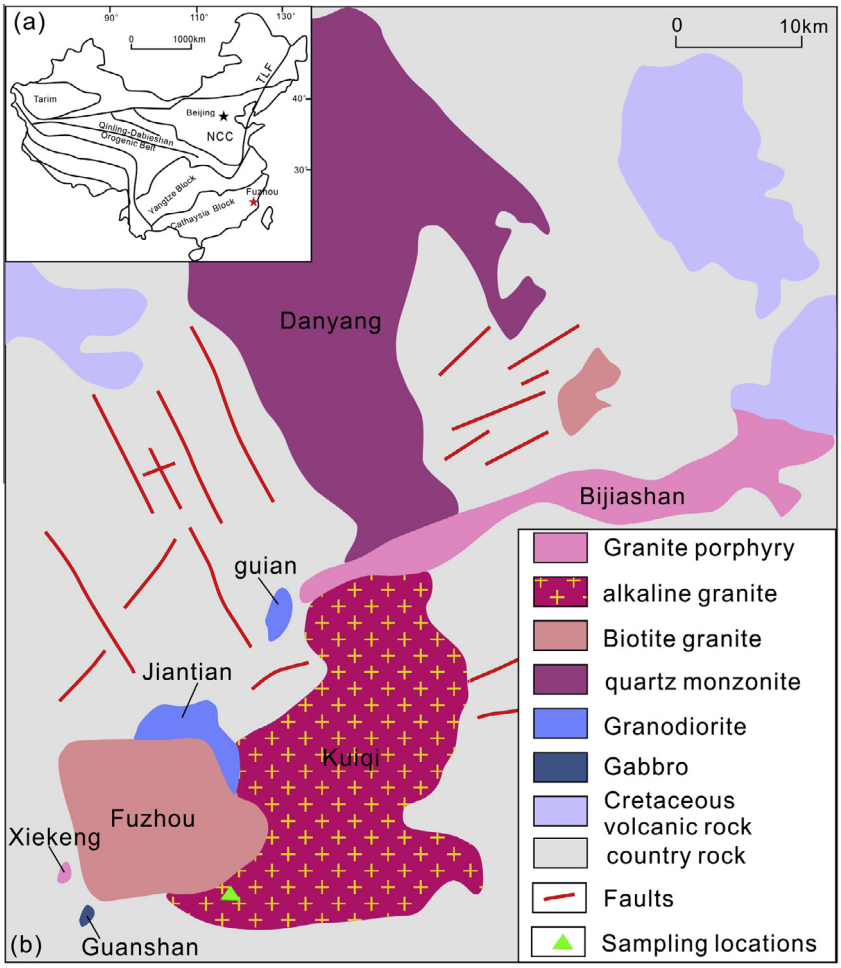

Fig. 1. (a) Regional geological map of China. (b) Simplified geologic map of the Kuiqi miarolite modified after Wu (1991). Abbreviations: NCC: North China Craton.

3.4. Fluid inclusion references

The salinities of aqueous fluid inclusions, expressed as wt.% NaCl equiv, were estimated using the formula of Bodnar (1994) for NaCl–H_2O system. The salinities of the halite daughter mineral-bearing inclusions were estimated using the methodology of Steele-MacInnis et al. (2012) based on the temperature of bubble dissolution and homogenization temperature.

4. Analytical results

4.1. Inclusion petrography

4.1.1. Inclusions types

Five primary inclusion types were identified based on the phases occurring at room temperature, phase change characteristics during heating, and laser Raman spectroscopy. Major characteristics of these five fluid inclusion types are summarized in Table 1 and described as follows:

(1) M-type (melt inclusion): M-type inclusions are commonly 20–50 μm in diameter. Some inclusions show apparent devitrification and/or network crystallization with blurry vapor (Fig. 3b), while others consist of glass, daughter minerals and bubbles (Fig. 3c). M-type inclusions are present in some quartz grains and rarely in the contact between the miarolitic quartz and the granite (Fig. 3a).

(2) ML type (melt–fluid inclusion): ML-type inclusions are mostly 15–60 μm in diameter, exhibiting variable size with different liquid/vapor/solids (except halite) ratios. They contain halite ± a highly birefringent phase (orthoclase, arfvedsonite, and quartz) (Fig. 3d and e). Occasionally an opaque phase can be observed. Microscopic measurements show that the vapor- and solid phases have accounted for about 10–25 vol.% and 10–50 vol.%, respectively. ML-type inclusions occur in clusters or are randomly distributed in the contact between the miarolitic quartz and the granite (Fig. 3a).

(3) S-type (daughter mineral-bearing) inclusions: the S-type inclusions occur mostly as negative crystal shapes and the vapor phase account for about 10–20 vol.%. They range from 10 to 50 μm in diameter and contain abundant daughter minerals such as halite, sylvite, and other unidentified daughter minerals (Fig. 3f and g). Halite is the dominant daughter mineral in the S-type inclusions. These inclusions are randomly distributed or occur in clusters in quartz grains of the granite. Most inclusions are distributed at the crystal bottom (Fig. 3a) and the middle of the miarolitic quartz (Fig. 3a).

(4) V-type (pure vapor or vapor-rich) inclusions: the inclusions consist of pure vapor and occasionally with <25 vol.% liquid (Fig. 3i). V-type inclusions commonly range from 20 to 40 μm in diameter, and are mainly elliptical in shape. Most inclusions are distributed at the crystal bottom in the miarolitic quartz. They are usually randomly distributed or occur in clusters, and are associated with M-, S- and L-type inclusions (Fig. 3h).

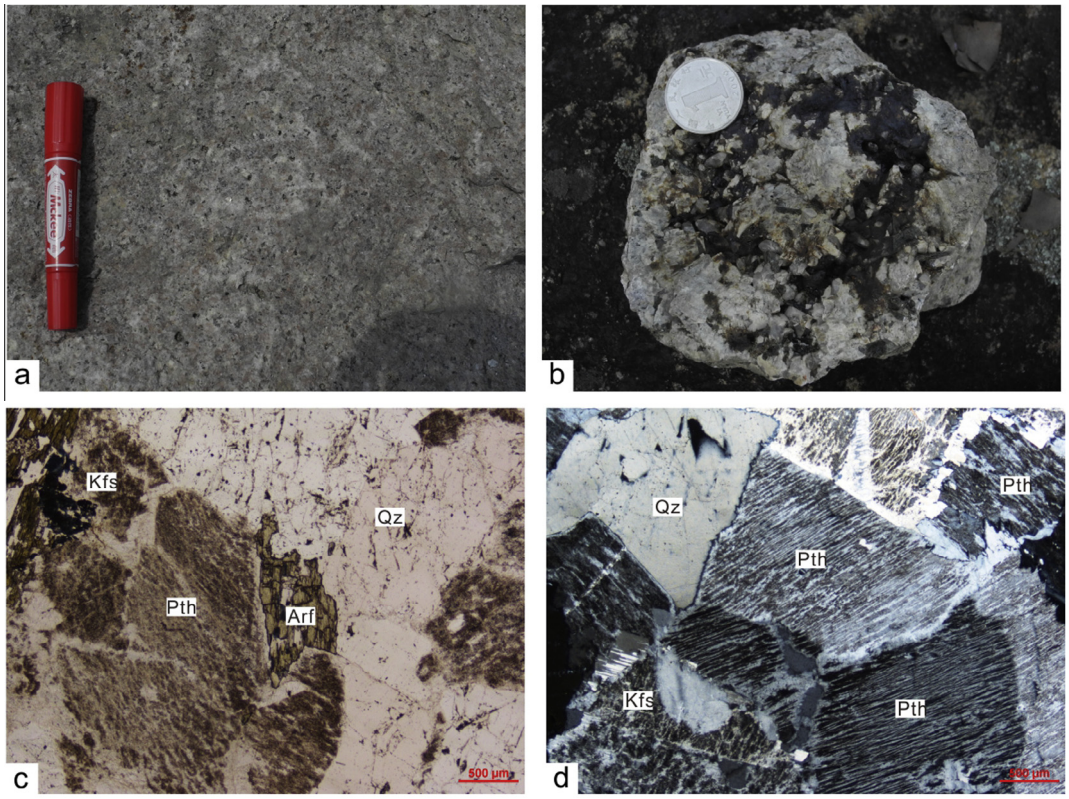

Fig. 2. Field photos and photomicrographs of the Kuiqi miarolite: (a) miarolitic granite; (b) miarolitic cavity; (c) miarolitic granite with perthitic texture; (d) arfvedsonite occurring in the interval of quartz and perthite. Abbreviations: Qz = quartz; Pth = perthite; Or = orthoclase; Arf = arfvedsonite. The diameter of the coin is 25 mm in (b).

Table 1
Overview of inclusion types of the Kuiqi miarolite.

Type	Fluid phases	Daughter minerals	Size (μm)	Vol.%	Shape	Occurrence
M		Arfvedsonite, quartz	20–50	5–15	Irregular	Isolated
ML		Halite, orthoclase, quartz, arfvedsonite	15–60	10–25	Irregular	Randomly distributed or in clusters
S	$V_{H_2O} + L_{H_2O}$	Halite, sylvite	10–50	10–20	Negative of elliptical	Randomly distributed or in clusters
V	$V_{H_2O} + L_{H_2O}$		20–40	<25	Negative or elliptical	Randomly distributed or in clusters
L	$V_{H_2O} + L_{H_2O}$		5–30	10–30	Negative or irregular	Randomly distributed, aligned or in clusters

Abbreviations: $V_{H_2}O$ = H_2O vapor; $L_{H_2}O$ = H_2O liquid; vol.% = volume percentage of the vapor phase.

(5) L-type (aqueous) inclusion: most L-type inclusions are 5–30 μm in diameter in negative or irregular crystals, showing two visible phases at room temperature (aqueous- and vapor H_2O). In general, the vapor has filling degrees (vapor phase proportion) of 5–30 vol.%. The filling degrees of the inclusions at the bottom (20–30 vol.%) (Fig. 3j) are higher than those at the top (10–15 vol.%) (Fig. 3k) of the miarolitic quartz. L-type inclusions are by far the most common type of inclusions, and are pervasively distributed either randomly, along planes or in clusters in the miarolitic cavities (Fig. 3a).

4.1.2. Inclusion assemblages

Inclusion assemblages commonly vary in different paragenetic stages (Ulrich et al., 2001; Ulrich and Heinrich, 2001). In this study, distribution of the inclusions in quartz from the miarolitic granites and cavities was documented to elucidate the magmatic evolution. Four inclusion assemblages were identified in the quartz grains of different magmatic evolution stages.

In the quartz grains from the granite, M-type inclusions constitute more than 60% of the total primary inclusion population, with the rest being The ML- (15%), S- (10%), V- (10%) and L- (5%) type inclusions.

Along the contact between the miarolitic quartz and the granite, M-type inclusions are abundant, whereas ML-type inclusions become predominant. Some M-type inclusions coexist with V-type inclusions (Fig. 4a). S- and L-type inclusions can be observed, but their abundance is less significant.

At the bottom and middle-low parts of the miarolitic quartz, S-type inclusions dominate, followed by the V-type and the high temperature L-type inclusions (Fig. 3h). Some S-type inclusions coexist with V-type inclusions (Fig. 4b).

At the top of the miarolitic quartz, only L-type inclusions of low filling degrees and low homogenization temperatures are present.

4.2. Microthermometric results

To elucidate the magmatic evolution, we analyzed different inclusion types in the quartz grains and the miarolitic quartz (from the bottom to the top).

4.2.1. Melt inclusions

To constrain the magmatic temperature, we analyzed the homogenization temperature of 16 melt inclusions in the quartz grains from the Kuiqi miarolitic granite (Fig. 5). We used stepped

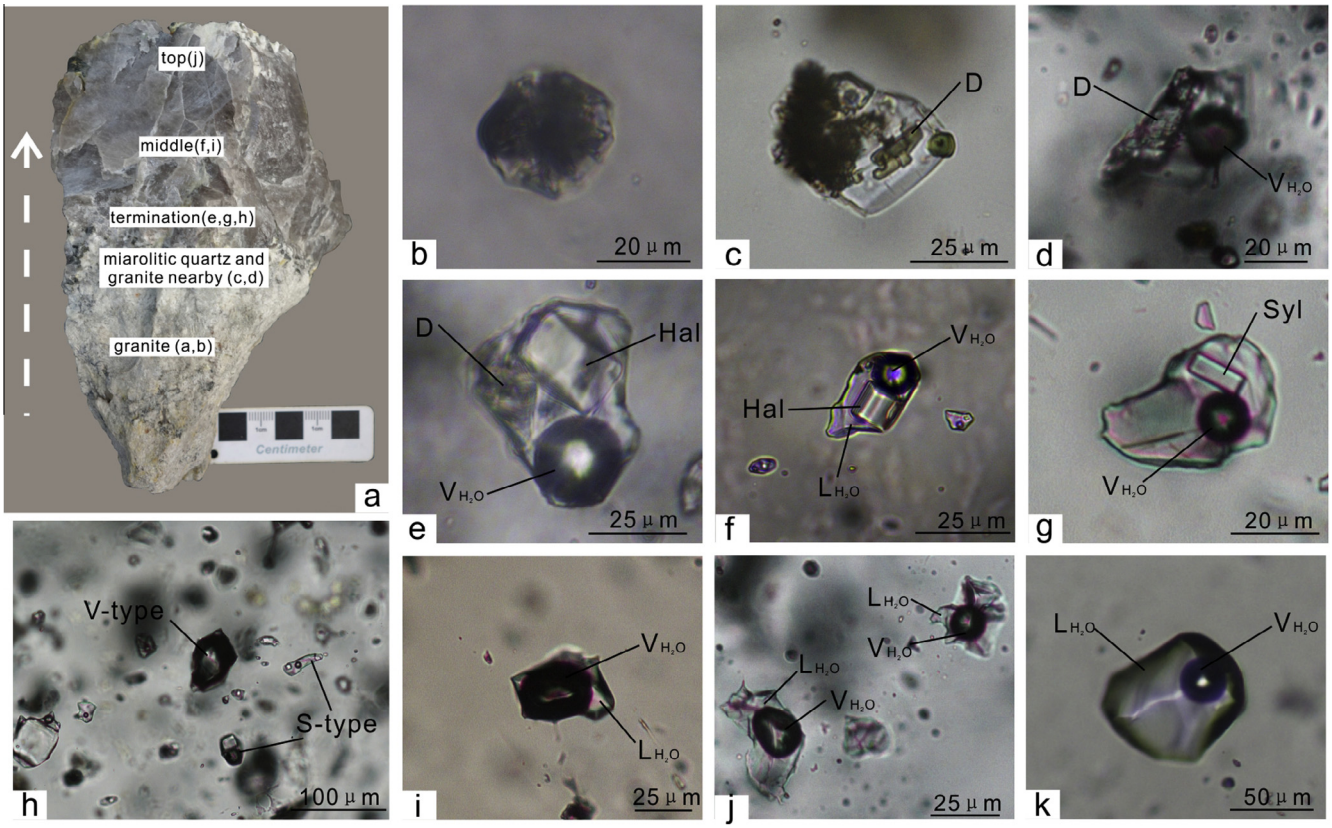

Fig. 3. Photomicrographs of the inclusions from the Kuiqi miarolite: (a) hand specimen of the miarolite. Note that the growth direction of the miarolite is indicated by the dash line arrow; (b) M-type inclusion with devitrification and network crystallization; (c) M-type inclusion with daughter mineral (arfvedsonite) and bubble; (d) ML-type inclusion with daughter mineral (orthoclase) and bubble; (e) ML-type inclusion with daughter mineral and halite; (f) S-type inclusion with halite; (g) S-type inclusion with sylvite; (h) S-type and V-type inclusions at the top of the miarolitic cavity; (i) V-type inclusion with V_{H_2O} and L_{H_2O}; (j) L-type inclusion with high filling degree at the middle part of the miarolitic cavity; (k) L-type inclusion with low filling degree at the top of the miarolitic cavity. Abbreviations: D = Daughter mineral; Hal = Halite; Syl = Sylvite; V_{H_2O} = H_2O vapor; L_{H_2O} = H_2O liquid

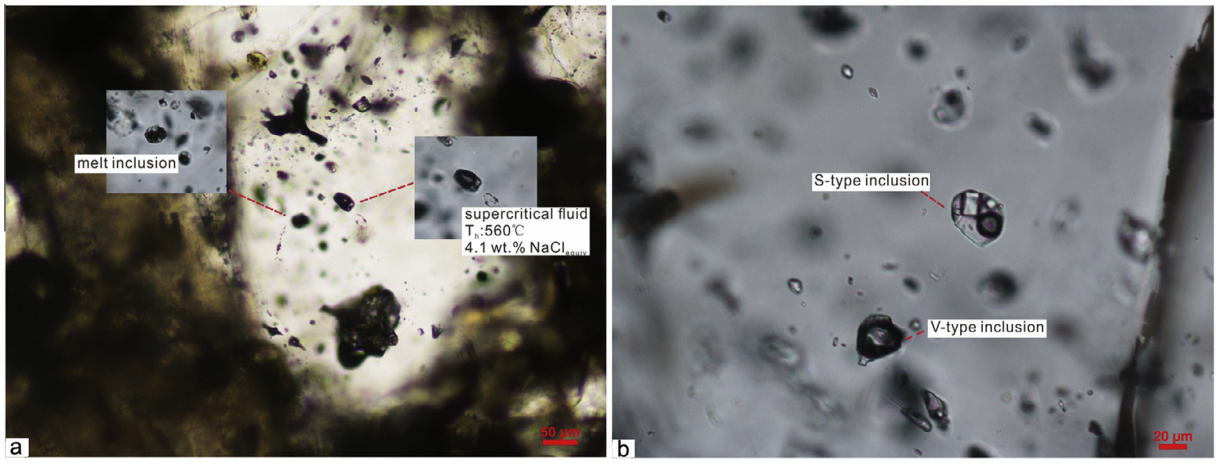

Fig. 4. (a) Coeval M- and V-type inclusions along the contact between the miarolitic quartz and the granite. (b) S-type inclusion coexists with V-type inclusion at the bottom of the miarolitic quartz.

heating method to homogenize the melt inclusions (Table 2). For example, the evolution of a crystallized melt inclusion as it was heated from room temperature up to 1120 °C is shown in Fig. 5. At 500 °C the inclusion became dark, and the bubbles shrank when the temperature reached to 700–800 °C. At 800 °C, the edge of the inclusion became smooth and the inclusion melted partially, and the bubbles agglomerated into a bigger one. With the heating resumed, the bubble got gradually smaller, and finally merged into a homogenized melt phase at 1120 °C. Quenching back to room temperature, the melt inclusion ford a homogenous glass and a vapor bubble, suggestive of a magmatic origin (Yang et al., 2011). Some melt inclusions did not homogenize even at temperatures up to 1200 °C. During the whole heating process, the field of view progressively darkened and a reddish glow developed, making it difficult to observe the melt inclusion behavior. Some melt inclusions decrepitated before homogenization, owing to the high

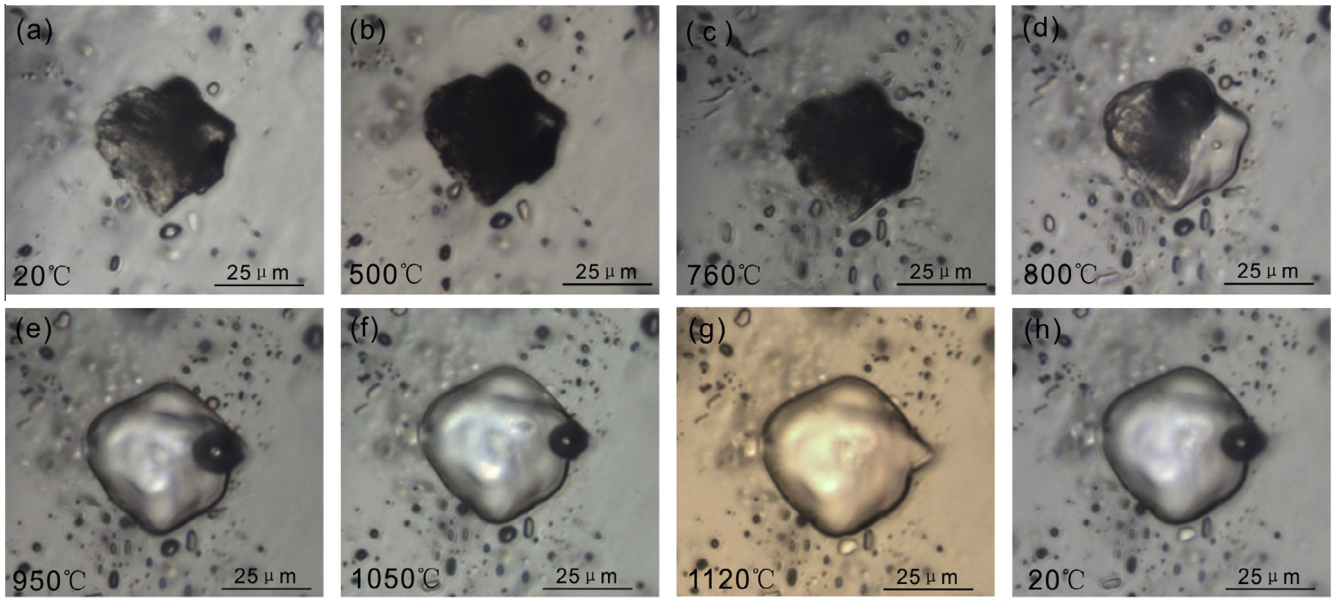

Fig. 5. Phase-change in the melt inclusion from the Kuiqi miarolite: (a) melt inclusion at room temperature; (b) the inclusion darkened; (c) the bubbles shrank and the inclusion began to get lighter; (d) inclusion began to melt and the bubbles agglomerated into one bubble; (e–f) the bubble got smaller and smaller; (g) the inclusion homogenized completely; (h) the bubble reappeared.

Table 2
Approximate heating rates for melt inclusions of the Kuiqi miarolite.

Sample	Inclusion size (μm)	Minor trapping temperature (°C)	Homogenization temperature (°C)	Heating rate (°C/min)
KQ-10-1	25	800	1150	
KQ-10-2	30	780	1150	
KQ-10-3	30	780	1200	
KQ-10-4	40	750	1200	
KQ-16-1	25	760	1160	
KQ-16-2	40	750	1150	
KQ-16-3	45	780	1200	Below 600 °C: 30 °C/min
KQ-16-4	30	750	1240	600–800 °C: 10 °C/min, holding 30 min at every 50 °C
KQ-17-1	35	740	1240	800–1000 °C: 5 °C/min, holding 1 h at every 50 °C
KQ-17-2	35	740	1120	1000 °C – homogenization: 5 °C, holding 2 h at every 50 °C
KQ-17-3	40	785	1120	
KQ-20-1	25	790	1120	
KQ-20-2	25	770	1150	
KQ-20-3	30	750	1250	
KQ-23-1	35	710	1200	
KQ-23-2	25	710	1150	
KQ-23-3	30	730	1150	
KQ-23-4	35	715	1150	

internal pressures. Thus, only 16 melt inclusions in this study reached the final homogenization (Table 2).

4.2.2. Melt–fluid inclusions

We were unable to obtain any homogenization temperature of the ML-type inclusions, because the internal pressures were so high that the inclusions decrepitated before reaching homogenization. Most ML-type inclusions decrepitated above 500 °C and thus their homogenization temperatures of ML-type inclusions are likely to be above 500 °C.

4.2.3. Fluid inclusions

Microthermometric results of the fluid inclusions are summarized in Table 3 and Fig. 6.

S-type inclusions show consistent homogenization behavior, i.e., halite dissolution subsequent to vapor bubble disappearance. The liquid–vapor homogenization by vapor bubble disappearance was observed at temperatures of 210–329 °C, and then the halite dissolution occured at temperatures from 275 °C to 485 °C, corresponding to salinities of 36.9–57.7 wt.% NaCl equiv. The salinities decreased from the bottom (45.6–57.7 wt.%) to middle (36.9–51.0 wt.%) of the quartz in the miarolitic cavities.

V-type inclusions exhibit the same microthermometric behavior of homogenization to vapor. The first melting temperatures of the V-type inclusions range from −27.8 to −24.6 °C, and the ice melting temperatures of these inclusions range from −6.7 to −4.9 °C. Homogenization of V-type inclusions occurred at temperatures from 352 to 540 °C, mostly in the range of 368–474 °C. Salinities of these inclusions range from 7.31 to 10.1 wt.% NaCl equiv.

L-type inclusions yielded first ice-melting temperatures from −29.1 to −23.4 °C, lower than the temperature of −21.2 °C and −22.9 °C determined for the H_2O–NaCl and H_2O–NaCl–KCl systems, respectively (Hall et al., 1988). The lower ice-melting temperatures indicate the presence of other ions besides Na^+ and K^+. Due to the lack of knowledge about fluids containing uncommon ions, the fluids in the L-type inclusions are approximated by the H_2O–NaCl–KCl system. The L-type inclusions in the miarolitic

Table 3
Microthermometric data of inclusions of the Kuiqi miarolite.

Type	Number	Ti (°C)	$T_{m,ice}$ (°C)	T_v (°C)	$T_{m,hal}$ (°C)	T_h (°C)	Salinity (wt.% NaCl)
ML	8					500–710	
S	38			210–329	275–485		36.9–57.7
V	12	−27.8 to −24.6	−6.7 to −4.9			352–540	7.31–10.1
L_1	48	−29.1 to −23.4	−14.1 to −4.1			303–427	6.6–17.9
L_2	45	−29.1 to −23.4	−3.5 to −0.1			165–232	0.2–5.7

Abbreviations: Ti (°C) = first ice-melting temperature; $T_{m,ice}$ (°C) = ice melting temperature; T_v (°C) = bubble disappearance temperature; $T_{m,hal}$ (°C) = melting temperature of halite; T_h (°C) = final homogenization temperature; L_1 = high homogenization temperature fluid inclusion; L_2 = low homogenization temperature fluid inclusion.

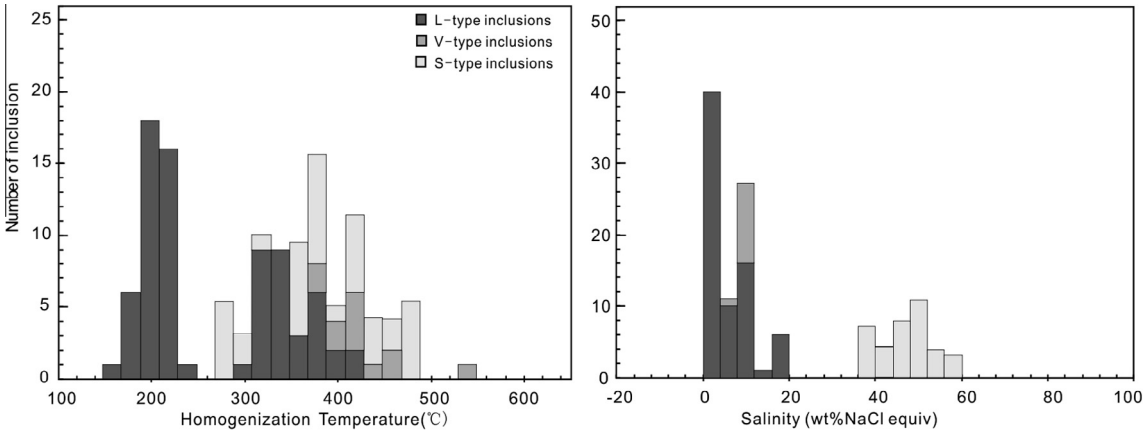

Fig. 6. Histograms of the homogenization temperatures and salinities of fluid inclusions from the Kuiqi miarolite.

quartz have a bimodal salinity distribution (Table 3). The high salinity inclusions (L_1) are distributed at the bottom and middle of the miarolitic quartz, with ice melting temperatures of −14.1 to −4.1°C, homogenization temperatures of 303–427 °C and corresponding salinities of 6.6–17.9 wt.% NaCl equiv. The low salinity inclusions (L_2) are distributed in the top of the miarolitic quartz, with ice melting temperatures of −3.5 to −0.1 °C, homogenization temperatures of 165–232 °C, and corresponding salinities of 0.2–5.7 wt.% NaCl equiv.

4.3. Laser Raman spectroscopy analysis

Representative inclusions were measured by laser Raman spectroscopy (LRM). The vapor phase compositions of ML-, V- and L-type inclusions are primarily water (peaks at 3748 cm^{-1}) (Fig. 7a). The spectrograms of the solid-phase in the melt–fluid inclusions suggest that the solid phase is dominated by orthoclase (peaks at 480 and 512 cm^{-1}) (Fig. 7b). A trace mineral phase, which could not be detected by LRM, is present in both M- and ML-type inclusions, yet petrographic observation suggests that is likely to be arfvedsonite.

5. Discussions

5.1. Magmatic stage

In Fig. 5, the melt inclusion changed obviously at 800 °C. Although the solids did not disappear completely, the residual solids have indistinguishable optical properties and show smooth contacts with the melt phases. This phenomenon may present evidence for residual solids being homogeneous composition minerals that melt at 800 °C. For the crystal mineral, it can be melted completely if the temperature at the melting point is maintained long enough (Yang et al., 2011). However, the inclusion can get completely homogenized in much shorter time when heated at higher temperatures. Therefore we consider that the minimal trapping temperature of the melt inclusion as shown in Fig. 4 is 800 °C. And the minimal trapping temperatures of the other 15 melt inclusions range from 710 to 790 °C (Table 2).

Magma of the Kuiqi miarolites may have been derived from partial melting of the Neoproterozoic lower crust with mantle input under an extensional tectonic setting which resulted from the subduction between the Kula and Eurasian plates (e.g., Shan et al., 2014). The minimal trapping temperatures of the Kuiqi melt inclusions range from 710 to 800 °C, suggesting that the quartz began to crystallize at these temperatures or higher. The graphic texture of the miarolite shows that the feldspar and quartz were crystallized simultaneously. These two minerals account for more than 90% of the granites, so this stage represent the major crystallization period. The zircon saturated temperatures (809–893 °C) estimated for the Kuiqi miarolites (Shan et al., 2014) are a little higher than the homogenization temperatures of the melt inclusions (Fig. 7), indicating that the crystallization of the magma initiated at temperatures no less than 800 °C.

Most melt inclusions in the granitic rocks show devitrification and some even contain mineral phases. Petrographic observations show that the mineral phases are arfvedsonites. M-type inclusions represent the melt entrapped at the magmatic crystallization stage. The presence of hydrous minerals in the inclusions, together with the abundant miarolitic cavities, suggest that the magma of the miarolitic granite was probably volatile-rich (Eggler, 1972).

5.2. Magmatic–hydrothermal stage

It is widely accepted that volatiles exsolved during crystallization of magmas (second boiling) bear significant amount of

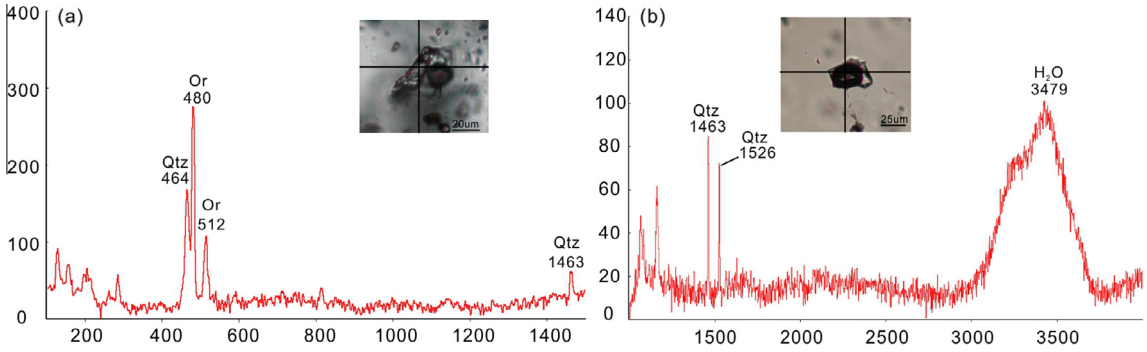

Fig. 7. Laser Raman spectra of fluid inclusions. (a) Orthoclase-spectra of the ML-type inclusion. (b) H_2O-spectra of the V-type inclusion. Abbreviations: Qtz = quartz; Or = orthoclase.

metallic elements (Candela and Holland, 1984; Harris et al., 2003; Kamenetsky et al., 1999; Robb, 2013; Shinohara, 1994; Webster, 1997). However, the record of fluids and their properties are usually either indirect or incomplete because of their transient nature. The coexistence of M- and V-type inclusions is a strong indication of volatile supersaturation, and the presence of ML-type inclusions confirms the existence of the transient of magmatic–hydrothermal stages.

Along the contact between the miarolitic quartz and granite, the ML-type inclusions with minimal trapping temperature of 715 °C coexist with low salinity (560 °C, 4.1 wt.% NaCl equiv) supercritical fluid inclusions of that depreciate at 630 °C (Fig. 4a). Even though the T_h of the V-type inclusion is difficult to obtain, it can be deduced that the total T_h should be lower than ca. 630 °C. Although homogenization temperature of the ML-type inclusions was not obtained, we can infer the homogenization temperature ML-type inclusions based on the homogenization temperature of the M-type and decrepitating temperature of the ML-type inclusions. The minimal trapping temperature of the M-type inclusion (710 °C) and the decrepitating temperature of the ML-type inclusion (above 500 °C) show that ML-type inclusions were probably entrapped at 500–710 °C. Thus, it can be inferred that magmatic supercritical fluids may have been exsolved from the crystallizing melt at this temperature.

According to the ternary phase diagrams of Or–Ab–Q, the magma evolving to the hydrothermal system should occur around the eutectic point of the granitic magma (Ernst, 1976). Abundant silicate minerals would crystallize from the melt and supercritical fluid phases would appear when the melt reaches saturation at the eutectic point. Audétat and Pettke (2003) discussed the magmatic–hydrothermal evolution of two barren granites in New Mexico. They found that the melt would be saturated before 30% crystallization and the evolved residual melt would accumulate in the magma chamber roof. At 90% crystallization, the melt would be supersaturated, and the fluid phases would appear. Ernst (1976) proposed that the Or–Ab–Q ternary point temperature ranges from 625 °C (10 kb) to 675 °C (3 kb). And the minimum trapping temperatures of the Kuiqi ML-type inclusions are 500–710 °C, indicating that the quartz hosting ML-type inclusions was formed at the magmatic to hydrothermal stage. The daughter minerals (arfvedsonite and orthoclase) and daughter crystals (halite) in ML-type inclusions are the same as those in the M- and S-type inclusions, respectively, which imply that ML-type inclusions were also formed at the magmatic–hydrothermal transition stage, representing the fluid exsolution.

The various proportions of bubble content in ML-type inclusions suggest that the they were formed through heterogeneous trapping. The distribution of M-, ML-, and S-type inclusions in the granitic rocks, as well as those at the bottom part of some quartz crystals in the miarolitic cavities, suggests that the immiscibility took place during the magmatic–hydrothermal transition stage, which is most likely near the solidus of the granitic system.

Both ML-type inclusions and the coexisting M- and V-type inclusions reflect the occurrence of magmatic fluids circulation toward at the end of fractionation and the magma-volatile immiscibility, which are typical features of the magmatic–hydrothermal transition stage (Frezzotti, 1992).

5.3. Hydrothermal stage

Inclusion results show that a high salinity fluid appeared in the miarolites at the temperature of about 485 °C. Most inclusions of the hydrothermal stage have halite and minor amounts of sylvite crystals. Their distribution and final homogenization temperatures suggest that high salinity brine circulation may have occurred at 275–485 °C. Total homogenization of S-type inclusions is characterized by halite disappearance. Some V-type inclusions coexisted with S-type inclusions at the top of the miarolitic cavity. The homogenization temperatures of the S-type and V-type inclusions are 410–474 °C and 385–447 °C, respectively (Fig. 4b). The V-type inclusions homogenization temperatures can be considered as the minimum estimation of the actual temperatures (Niu and Lin, 1995; Niu et al., 1997). Given that the two inclusion types have approximately identical homogenization temperature ranges while homogenized into different phases, it can be inferred that segregation may have occurred locally at this stage (Fig. 8). At the early stage of the hydrothermal evolution, both pressure and temperature (700–485 °C) of the intrusions drop, and the primary salinity fluid becomes saturated and separates into two phases at the end of crystallization, i.e., high salinity fluids and volatile-rich fluids, leading to widespread vapor–brine immiscibility (Audétat et al., 2008; Ramboz et al., 1982; Shan et al., 2011). Numerous boiling assemblages document that at temperatures of 400 °C and 600 °C the fluid was mostly in the two-phase field (Audétat and Pettke, 2003; Jiang et al., 2014)

As aforementioned, L-type inclusions include high salinity- and low salinity members. The high salinity L-type inclusions are distributed at the top to middle of the miarolitic quartz with higher filling degree, whereas the low salinity ones are mainly distributed at the middle to top of the miarolitic quartz with lower filling degree.

The H_2O fluid exsolution from the magmas is commonly accompanied by the release of mechanical energy, since the volume per unit mass of the silicate melts plus the low density H_2O is greater than the equivalent mass of H_2O saturated magma (Burnham, 1979). This results in overpressuring of the magma chamber interior and may cause brittle deformation of the country rocks. The hydrofracturing that results from this type of failure usually forms

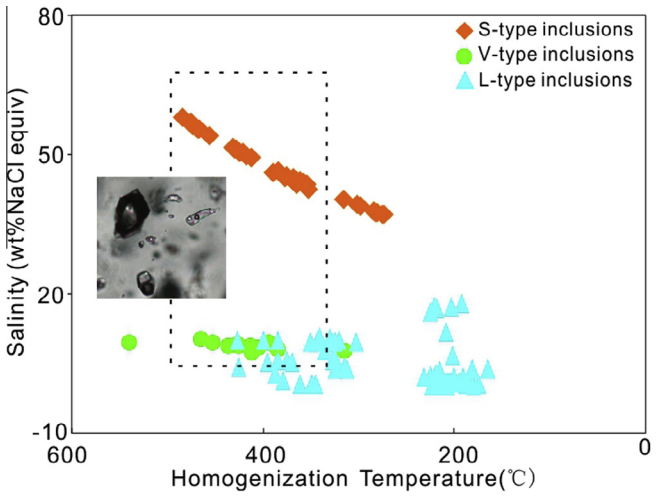

Fig. 8. Homogenization temperatures *vs.* salinities of fluid inclusions. Some coexisting S-type and V-type inclusions have similar homogenization temperatures and show immiscible features. The region inside the dashed rectangle shows the range of salinities and homogenization temperatures measured for the S-, V- and L_1-type inclusions.

fractures which provide access of the meteoric water to the magma chamber. At the early stage of the hydrothermal evolution, the temperature of the magma were so high that the meteoric water evaporated and couldn't enter into the magma chamber. But at the late stage of the hydrothermal evolution, with the decreasing of temperature, the heat barrier disappeared that the meteoric water participated in the evolution.

So the low homogenization temperatures and salinity of L-type inclusions indicate the meteoric water influx at the late stage of hydrothermal evolution (Audétat et al., 2008; Jiang et al., 2014). Thus, it is clear that the filling degrees of the vapor, temperature and salinity of the fluids decrease from the bottom to the top of the miarolitic quartz (Fig. 8).

5.4. Geological significance

Experimental works suggested that high level intrusion is capable of facilitating brittle deformation, both in the intrusion itself and in the surrounding country rocks, thereby providing excellent ground preparation for the efficient circulation of ore-bearing fluids (Dingwell et al., 1997). The factors that help to promote brittle failure in high level granite-related ore-forming systems include volatile saturation (Robb, 2013), bubble vesiculation, and rapid cooling.

When volatiles are exsolved from the parental magmas, immiscibility generates a separate volatile-rich phase and leads to a major change in the element partitioning (Kamenetsky et al., 2004). It is considered that volatile phase exsolved during the crystallization of magmas carry significant amounts of metallic elements. If dense, these phases may precipitate in situ (e.g., Fe–Cu–Ni–PGE sulfides); if buoyant, they may enter hydrothermal systems and be responsible for formation of certain types of ore deposits (e.g., W–Sn skarns and greisens, pegmatites). Kamenetsky et al. (2004) studied inclusions in phenocrystic and miarolitic quartz from the Omsukchan granite (NE Russia) and found that exsolution of the volatile element-rich phase from cooling and crystallising silicate magmas is critical for element transport from the Earth's interior into the atmosphere, hydrosphere, crustal hydrothermal systems, and the formation of orthomagmatic ore deposits.

The geological consequences of brine–vapor separation are considered as a mechanism to segregate elements and selectively enrich certain metals in different types of ore deposits. "Boiling" is an important process driving precious-metal deposition in epithermal deposits (Drummond and Ohmoto, 1985). Brine and vapor not only have contrasting densities, but also vastly different viscosities. These contrasts in physical properties will facilitate the separation of big volumes of fluids and promote large-scale selective element transport, particularly in the dynamic environment of magmatic–hydrothermal systems in continental and submarine setting (Heinrich et al., 1999).

Heinrich et al. (1999) demonstrated that unambiguous evidence for coeval trapping of a liquid brine and a coexisting vapor phase, and identified two groups of elements with drastically different geochemical behavior: Na, K, Fe, Mn, Zn, Rb, Cs, Ag, Sn, Pb and Tl preferentially partition into the brine (probably as Cl complexes), whereas Cu, As, Au (probably as HS complexes) and B selectively partition into the vapor.

The Kuiqi miarolites experienced a complete magmatic evolution: Magmatic melt → Melt and low salinity fluid → High salinity fluid → Low salinity fluid. The magma may have evolved from volatile-rich to volatile saturation and eventually to supersaturation. Two immiscible phenomenons, which are important factors for the metallic transportation and concentration, occur in the process: volatile–magma and brine–vapor.

6. Conclusions

(1) M-type inclusions represent the melt entrapped during crystallization, in addition, the occurrence of euhedral arfvedsonites prismatic crystals in the melt inclusions indicates that the primary magma was probably volatile-rich.
(2) Both ML-type inclusions and the coexisting M- and V-type inclusions reflect the occurrence of magmatic fluids circulation (toward the end of crystallization) and the magma-volatile immiscibility, characterizing the transition to the hydrothermal stage.
(3) With the drop of pressure and temperature at the early stage of the hydrothermal evolution stage, the primary saline fluids may have become saturated and separated into two phases, i.e., high salinity fluids and volatile-rich fluids, leading to widespread vapor–brine immiscibility.
(4) The bimodal distribution of the L-type inclusions in the miarolitic quartz suggests that the filling degrees of the vapor, temperature and salinity of the fluid decrease from the bottom to the top of the miarolitic quartz, and the low homogenization temperatures and salinity of L-type inclusions reflect the participation of meteoric water at the late stage of the hydrothermal evolution.

Acknowledgments

This study was financially supported by the National Nature Science Foundation of China grants (41373031 and 41472062). We sincerely thank the staffs of the Key Laboratory of Mineralogy and Metallogeny (GIGCAS) for their substantial assistance during the laboratory works. We are grateful to the two anonymous reviewers for constructive comments that helped improve the manuscript substantially. This is contribution No. IS-2227 from GIGCAS.

References

Audétat, A., 2015. Compositional evolution and formation conditions of magmas and fluids related to porphyry mo mineralization at climax, Colorado. J. Petrol., egv044

Audétat, A., Pettke, T., 2003. The magmatic–hydrothermal evolution of two barren granites: a melt and fluid inclusion study of the Rito del Medio and Cañada Pinabete plutons in northern New Mexico (USA). Geochim. Cosmochim. Acta 67, 97–121.

Audétat, A., Pettke, T., Heinrich, C.A., Bodnar, R.J., 2008. Special paper: the composition of magmatic–hydrothermal fluids in barren and mineralized intrusions. Econ. Geol. 103, 877–908.

Badanina, E., Veksler, I., Thomas, R., Syritso, L., Trumbull, R., 2004. Magmatic evolution of Li–F, rare-metal granites: a case study of melt inclusions in the Khangilay complex, Eastern Transbaikalia (Russia). Chem. Geol. 210, 113–133.

Bai, Z.J., Zhu, W.G., Zhong, H., Li, C., Liao, J.Q., Sun, H.S., 2015. Petrogenesis and tectonic implications of the early Jurassic Fe–Ti oxide-bearing Xialan mafic intrusion in SE China: constraints from zircon Hf–O isotopes, mineral compositions and whole-rock geochemistry. Lithos 212, 59–73.

Bakker, R.J., Elburg, M.A., 2006. A magmatic–hydrothermal transition in Arkaroola (northern Flinders Ranges, South Australia): from diopside–titanite pegmatites to hematite–quartz growth. Contrib. Miner. Petrol. 152, 541–569.

Barnes, H.L., 1997. Geochemistry of Hydrothermal Ore Deposits. John Wiley and Sons, New York, p. 422.

Bodnar, R.J., 1994. Synthetic fluid inclusions. XII: the system H_2O–NaCl. Experimental determination of the halite liquidus and isochors for a 40% NaCl solution. Geochim. Cosmochim. Acta 58, 1053–1063.

Burnham, C.W., 1979. The importance of volatile constituents. In: Yoder, H.S.J. (Ed.), The Evolution of the Igneous Rocks. Princeton University Press, Princeton, NJ, pp. 439–482.

Candela, P.A., Holland, H.D., 1984. The partitioning of copper and molybdenum between silicate melts and aqueous fluids. Geochim. Cosmochim. Acta 48, 373–380.

Cathelineau, M., Dubessy, J., Marignac, C., Poty, B., Weisbrod, A., 1988. Fluids in granitic environment. Rendiconti – Sociea Italiana di Mineralogia e Petrologia 43, 263–274.

Cui, J., Zhang, Y., Dong, S., Jahn, B.-M., Xu, X., Ma, L., 2013. Zircon U–Pb geochronology of the Mesozoic metamorphic rocks and granitoids in the coastal tectonic zone of SE China: constraints on the timing of Late Mesozoic orogeny. J. Asian Earth Sci. 62, 237–252.

Dingwell, D., Holtz, F., Behrens, H., 1997. The solubility of H_2O in peralkaline and peraluminous granitic melts. Am. Mineral. 82, 434–437.

Drummond, S., Ohmoto, H., 1985. Chemical evolution and mineral deposition in boiling hydrothermal systems. Econ. Geol. 80, 126–147.

Eggler, D.H., 1972. Amphibole stability in H_2O-undersaturated calc-alkaline melts. Earth Planet. Sci. Lett. 15, 28–34.

Ernst, W.G., 1976. Petrologic Phase Equilibria. Freeman, San Francisco, pp. 126–128.

Esposito, R., Klebesz, R., Bartoli, O., Klyukin, Y.I., Moncada, D., Doherty, A.L., Bodnar, R.J., 2012. Application of the Linkam TS1400XY heating stage to melt inclusion studies. Cent. Eur. J. Geosci. 4, 208–218.

Fan, H.R., Liu, J.B., Guo, J.H., Ye, K., Cong, B.L., 2002. Fluid inclusions in whiteschist in the ultrahigh-pressure metamorphic belt of Dabie Shan, China. Chin. Sci. Bull. 47, 1028–1032.

Fan, H.R., Zhai, M.G., Xie, Y.H., Yang, J.H., 2003. Ore-forming fluids associated with granite-hosted gold mineralization at the Sanshandao deposit, Jiaodong gold province, China. Miner. Deposita 38, 739–750.

Frezzotti, M.L., 1992. Magmatic immiscibility and fluid phase evolution in the Mount Genis granite (southeastern Sardinia, Italy). Geochim. Cosmochim. Acta 56, 21–33.

Gruen, G., Weis, P., Driesner, T., Heinrich, C.A., de Ronde, C.E.J., 2014. Hydrodynamic modeling of magmatic–hydrothermal activity at submarine arc volcanoes, with implications for ore formation. Earth Planet. Sci. Lett. 404, 307–318.

Hall, D.L., Sterner, S.M., Bodnar, R.J., 1988. Freezing point depression of NaCl–KCl–H_2O solutions. Econ. Geol. 83, 197–202.

Hammerli, J., Rusk, B., Spandler, C., Emsbo, C., Oliver, N.H., 2013. In situ quantification of Br and Cl in minerals and fluid inclusions by LA-ICP-MS: a powerful tool to identify fluid sources. Chem. Geol. 337, 75–87.

Hansteen, T., Lustenhouwer, W., 1990. Silicate melt inclusions from a mildly peralkaline granite in the Oslo paleorift, Norway. Mineral. Mag. 54, 195–205.

Harris, A.C., Kamenetsky, V.S., White, N.C., van Achterbergh, E., Ryan, C.G., 2003. Melt inclusions in veins: linking magmas and porphyry Cu deposits. Science 302, 2109–2111.

Heinrich, C., Günther, D., Audétat, A., Ulrich, T., Frischknecht, R., 1999. Metal fractionation between magmatic brine and vapor, determined by microanalysis of fluid inclusions. Geology 27, 755–758.

Heinrich, C.A., Pettke, T., Halter, W.E., Aigner-Torres, M., Audétat, A., Günther, D., Hattendorf, B., Bleiner, D., Guillong, M., Horn, I., 2003. Quantitative multi-element analysis of minerals, fluid and melt inclusions by laser-ablation inductively-coupled-plasma mass-spectrometry. Geochim. Cosmochim. Acta 67, 3473–3497.

Huang, X., Sun, S., DePaolo, D., Wu, K., 1986. Nd–Sr isotope study of Cretaceous magmatic rocks from Fujian province. Acta Petrologica Sinica 2, 50–63 (in Chinese with English abstract).

Hurtig, N.C., Heinrich, C.A., Driesner, T., Herrmann, W., Wall, V., Mathison, I., 2014. Fluid evolution and uranium (–Mo–F) mineralization at the Maureen Deposit (Queensland, Australia): unconformity-related hydrothermal ore formation with a source in the volcanic cover sequence. Econ. Geol. 109, 737–773.

Jiang, Y.H., Niu, H.C., Bao, Z.W., Li, N.B., Shan, Q., Yang, W.B., 2014. Fluid evolution of the Tongkuangyu porphyry copper deposit in the Zhongtiaoshan region: evidence from fluid inclusions. Ore Geol. Rev. 66, 498–509.

Kamenetsky, V.S., Kamenetsky, M.B., 2010. Magmatic fluids immiscible with silicate melts: examples from inclusions in phenocrysts and glasses, and implications for magma evolution and metal transport. Geofluids 10, 293–311.

Kamenetsky, V.S., Naumov, V.B., Davidson, P., Van Achterbergh, E., Ryan, C.G., 2004. Immiscibility between silicate magmas and aqueous fluids: a melt inclusion pursuit into the magmatic–hydrothermal transition in the Omsukchan Granite (NE Russia). Chem. Geol. 210, 73–90.

Kamenetsky, V.S., Wolfe, R.C., Eggins, S.M., Mernagh, T.P., Bastrakov, E., 1999. Volatile exsolution at the Dinkidi Cu–Au porphyry deposit, Philippines: a melt-inclusion record of the initial ore-forming process. Geology 27, 691–694.

Kurosawa, M., Shimano, S., Ishii, S., Shima, K., Kato, T., 2003. Quantitative trace element analysis of single fluid inclusions by proton-induced X-ray emission (PIXE): application to fluid inclusions in hydrothermal quartz. Geochim. Cosmochim. Acta 67, 4337–4352.

Lawrence, D.M., Treloar, P.J., Rankin, A.H., Boyce, A., Harbidge, P., 2013. A fluid inclusion and stable isotope study at the Loulo mining district, Mali, West Africa: Implications for multifluid sources in the genertion of orogenic gold deposits. Econ. Geol. 108, 229–257.

Li, N., Ulrich, T., Chen, Y.J., Thomsen, T.B., Pease, V., Pirajno, F., 2012. Fluid evolution of the Yuchiling porphyry Mo deposit, East Qinling, China. Ore Geol. Rev. 48, 442–459.

Lu, H.Z., 2011. Fluids immiscibility and fluid inclusions. Acta Petrologica Sinica 27, 1253–1261 (in Chinese with English abstract).

Lu, H.Z., Liu, Y.M., Wang, C.L., Xu, Y.Z., Li, H.Q., 2003. Mineralization and fluid inclusion study of the Shizhuyuan W–Sn–Bi–Mo–F skarn deposit, Hunan province, China. Econ. Geol. 98, 955–974.

Martin, H., Bonin, B., Jahn, B.M., Lameyre, J., Wang, Y., 1994. The Kuiqi peralkaline granitic complex (SE China): petrology and geochemistry. J. Petrol. 35, 983–1015.

Mogdisov, Art.A., Williams-Jones, A.E., 2013. A predictive model for metal transport of silver chloride by aqueous vapor in ore-forming magmatic–hydrothermal systems. Geocheimica et Cosmochimica Acta 104, 123–135.

Morales, M.J., e Silva, R.C.F., Lobato, L.M., Gomes, S.D., Gomes, C.C., Banks, D.A., 2016. Metal source and fluid–rock interaction in the Archean BIF-hosted Lamego gold mineralization: microthermometric and LA-ICP-MS analyses of fluid inclusions in quartz veins, Rio das Velhas greenstone belt, Brazil. Ore Geol. Rev. 72, 510–531.

Niu, H.C., Lin, C.X., 1995. Study on the fluid–melt inclusions in fluorite. Geol. Rev. 1, 28–33 (in Chinese with English abstract).

Niu, H.C., Shan, Q., Chen, P.R., 1997. Study of fluid properties on magmatic–hydrothermal stage: a case study of Mianning REE Deposit, Sichuan. J. Nanjing Univ. (Nat. Sci.) 33, 21–27 (in Chinese with English abstract).

Ramboz, C., Pichavant, M., Weisbrod, A., 1982. Fluid immiscibility in natural processes: use and misuse of fluid inclusion data II: interpretation of fluid inclusion data in terms of immiscibility. Chem. Geol. 37, 29–48.

Robb, L., 2013. Introduction to Ore-forming Processes. John Wiley & Sons, p. 85.

Poros, Z., Mindszenty, A., Molnár, F., Pironon, J., Győri, O., Ronchi, P., Szekeres, Z., 2012. Imprints of hydrocarbon-bearing basinal fluids on a karst system: mineralogical and fluid inclusion studies from the Buda Hills, Hungary. Int. J. Earth Sci. 101, 429–452.

Roedder, E., 1984. Fluid inclusions. Miner. Soc. Am. Rev. Miner. 12, 644.

Shan, Q., Liao, S.P., Lu, H.Z., Li, J.K., Yang, W.B., Luo, Y., 2011. Fluid inclusion records from the magmatic to hydrothermal stage: a case study of Qitianling granite pluton. Acta Petrologica Sinica 27, 1511–1520 (in Chinese with English abstract).

Shan, Q., Zeng, Q.S., Li, J.K., Lu, H.Z., Hou, M.Z., Yu, X.Y., Wu, C.J., 2014. U–Pb geochronology of zircon and geochemistry of Kuiqi miarolitic granites, Fujian province. Acta Petrologica Sinica 30, 1155–1167 (in Chinese with English abstract).

Shinohara, H., 1994. Exsolution of immiscible vapor and liquid phases from a crystallizing silicate melt: implications for chlorine and metal transport. Geochim. Cosmochim. Acta 58, 5215–5221.

Sillitoe, R.H., 2010. Porphyry copper systems. Econ. Geol. 105, 3–41.

Sirbescu, M.-L.C., Krukowski, E.G., Schmidt, C., Thomas, R., Samson, I.M., Bodnar, R.J., 2013. Analysis of boron in fluid inclusions by microthermometry, laser ablation ICP-MS, and Raman spectroscopy: application to the Cryo-Genie Pegmatite, San Diego county, California, USA. Chem. Geol. 342, 138–150.

Steele-MacInnis, M., Lecumberri-Sanchezm, P., Bodnar, R.J., 2012. $HOKIEFLINCS\_H_2O$–N_AC_L: a Microsoft Excel spreadsheet for interpreting microthermometric data from fluid inclusions based on the PVTX properties of H_2O–NaCl. Comput. Geosci. 49, 334–337.

Suwa, K., Enami, M., Hiraiwa, I., Yang, T.M., 1987. Zn–Mn ilmenite in the Kuiqi Granite from Fuzhou, Fujian Province, East China. Mineral. Petrol. 36, 111–120.

Thomas, R., Davidson, P., Beurlen, H., 2012. The competing models for the origin and internal evolution of granitic pegmatites in the light of melt and fluid inclusion research. Mineral. Petrol. 106, 55–73.

Thomas, R., Davidson, P., Rhede, D., Leh, M., 2009. The miarolitic pegmatites from the Konigshain: a contribution to understanding the genesis of pegmatites. Contrib. Miner. Petrol. 157, 505–523.

Ulrich, T., Gunther, D., Heinrich, C.A., 2001. The evolution of a porphyry Cu–Au deposit, based on LA-ICP-MS analysis of fluid inclusions: Bajo de la Alumbrera, Argentina. Econ. Geol. Bull. Soc. Econ. Geol. 96, 1743–1774.

Ulrich, T., Heinrich, C.A., 2001. Geology and alteration geochemistry of the porphyry Cu–Au deposit at Bajo de la Alumbrera, Argentina. Econ. Geol. Bull. Soc. Econ. Geol. 96, 1719–1742.

Wang, D.Z., Peng, Y.M., Yuan, P., 1985. Petrology, geochemistry and genesis of Kuiqi granite batholith. Geochimica 3, 197–205 (in Chinese with English abstract).

Webster, J.D., 1997. Exsolution of magmatic volatile phases from Cl-enriched mineralizing granitic magmas and implications for ore metal transport. Geochim. Cosmochim. Acta 61, 1017–1029.

Weisbrod, A., 1981. Fluid inclusions in shallow intrusives. Fluid Inclusions: Application to Petrology, vol. 7. Mineralogical Association of Canada, Ottawa, pp. 241–271 (Short course).

Wu, G.Q., 1991. The compositions and evolution of Fuzhou composite intrusion. Acta Petrologica Sinica 2, 81–88 (in Chinese with English abstract).

Xie, Y.L., Hou, Z.Q., Yin, S.P., Dominy, S.C., Xu, J.H., Tian, S.H., Xu, W.Y., 2009. Continuous carbonatitic melt–fluid evolution of a REE mineralization system: evidence from inclusions in the Maoniuping REE Deposit, Western Sichuan, China. Ore Geol. Rev. 36, 90–105.

Yang, K., Bodnar, R.J., 1994. Magmatic–hydrothermal evolution in the "Bottoms" of porphyry copper systems: evidence from silicate melt and aqueous fluid inclusions in granitoid intrusions in the Gyeongsang basin, South Korea. Int. Geol. Rev. 36, 608–628.

Yang, W.B., Su, W.C., Liao, S.P., Niu, H.C., Luo, Y., Shan, Q., Li, N.B., 2011. Melt and melt–fluid inclusions in the Baerzhe alkaline granite: information of the magmatic–hydrothermal transition. Acta Petrologica Sinica 27, 1493–1499 (in Chinese with English abstract).

Zhou, J., Jiang, Y.H., Xing, G., Zeng, Y., Ge, W., 2013. Geochronology and petrogenesis of Cretaceous A-type granites from the NE Jiangnan Orogen, SE China. Int. Geol. Rev. 55, 1359–1383.